

# Alignment based on a ‘no adjustment’ philosophy for the Immersion Grating Infrared Spectrometer (IGRINS)

Jeong-Yeol Han<sup>a</sup>, In-Soo Yuk<sup>a,b</sup>, Kyeongyeon Ko<sup>a</sup>, Heeyoung Oh<sup>a</sup>, Jakyoungh Nah<sup>a</sup>, Jae Sok Oh<sup>a</sup>, Chan Park<sup>a</sup>, Sungho Lee<sup>b</sup>, Kang-Min Kim<sup>a</sup>, Moo-Young Chun<sup>a</sup>, Daniel T. Jaffe<sup>c</sup>, Soojong Pak<sup>d</sup>, Michael Gully-Santiago<sup>c</sup>

<sup>a</sup>Korea Astronomy and Space Science Institute, Daejeon, Korea

<sup>b</sup>SELab Inc., Seoul, Korea

<sup>c</sup>The University of Texas at Austin, USA

<sup>d</sup>Kyung Hee University, Suwon, Korea

## ABSTRACT

IGRINS, the Immersion GRating INfrared Spectrometer includes an immersion grating made of silicon and observes both H-band (1.49~1.80  $\mu\text{m}$ ) and K-band (1.96~2.46  $\mu\text{m}$ ), simultaneously. In order to align such an infrared optical system, the compensator in its optical components has been adjusted within tolerances at room temperature without vacuum environment. However, such a system will ultimately operate at low temperature and vacuum with no adjustment mechanism. Therefore a reasonable relationship between different environmental variations such as room and low temperature might provide useful knowledge to align the system properly. We are attempting to develop a new process to predict the Wave Front Error (WFE), and to produce correct mechanical control values when the optical system is perturbed by moving the lens at room temperature. The purpose is to provide adequate optical performance without making changes at operating temperature. In other words, WFE was measured at operating temperature without any modification but a compensator was altered correctly at room temperature to meet target performance. The ‘no adjustment’ philosophy was achieved by deterministic mechanical adjustment at room temperature from a simulation that we developed. In this study, an achromatic doublet lens was used to substitute for the H and K band camera of IGRINS. This novel process exhibits accuracy predictability of about 0.002  $\lambda$  rms WFE and can be applied to a cooled infrared optical systems.

Keywords: Alignment, Assembly, IGRINS, Immersion grating, No adjustment, WFE

## 1. INTRODUCTION

Most infrared optical systems work in low temperature (LT) and vacuum (V) environments but assembly and alignment for these systems is usually done under room temperature (RT) and non-vacuum (NV) conditions because an adjustment of optical components at both RT and NV conditions is relatively easier than at low temperature and under vacuum<sup>1-4</sup>. In addition, optical performance at LT differs substantially results from that at RT due to changing physical properties<sup>5,6</sup> such as radius of curvature ( $rc$ ), thickness ( $t$ ) and decentering ( $dc$ ) of optical components. Therefore an ability to predict appropriate mechanical adjustment quantities at RT in order to provide the required optical performance at Operating Temperature (OT) could provide us with a practical tool to determine the correct alignment for cryogenic infrared optical systems.

IGRINS<sup>7</sup> is a high-resolution ( $\lambda/\delta\lambda \sim 40000$ ) infrared spectrograph operated in cryogenic temperature (130 K) and vacuum environments, under development since 2008. In order to properly assemble such an infrared instrument at RT, a ‘no adjustment’ philosophy has been proposed<sup>8-14</sup>. For example, MIRI<sup>8</sup> was aligned within mechanical tolerances using sensitivity analysis, and both MIDI<sup>9,10</sup> and VISIR<sup>11</sup> adopted the philosophy of adjusting a mirror and a detector or wheel. MATISSE<sup>12-14</sup> adjusted in part using a piezo-driven adjustment mechanism<sup>14</sup>. Among the infrared instruments developed such as Planck<sup>15</sup>, Herschel<sup>16</sup>, the Volume Phase Holographic Gratings (VPHGs)<sup>17</sup>, C/SiC optics for SPICA<sup>18</sup>, and the Near Infrared Camera (NIC)<sup>19</sup> and near infrared spectrograph (NIRSpec)<sup>20</sup> of JWST have been aligned and have obtained optical performance without implementing such a philosophy of prediction simulation. For instance, Planck reflectors<sup>15</sup>

composed of 2 carbon-fiber-reinforced-polymer (CFRP) off-axis ellipsoids have been tested in cryogenic conditions to measure the surface figure error (SFE), in order to compare performance between RT and OT. The Spectral and Photometric Imaging REceiver (SPIRE) in Herschel<sup>16</sup> used pupil alignment methodology. We could not find adequate examples to simulate predictable WFE as a performance indicator for such a ‘no adjustment’ philosophy. Nevertheless, WFE is predictable and able to be controlled precisely.

In this study, we used WFE as a performance indicator and the WFE was simulated by the prediction algorithm we developed. Besides providing this indicator, the developed simulation indicated the level of mechanical adjustment at RT in order to meet required optical performance at OT without any adjustment. The predicted WFE was compared with experimental results. Chapter 2 describes the simulation flow and the experimental confirmation procedure is summarized in Chapter 3. Chapters 4 and 5 provide validated results and conclusions.

## 2. SIMULATION FLOW

In order to simplify the optical configuration for verification of simulation results, we adopted an achromatic doublet lens with optical specifications similar to those of the H-band (1.49~1.80 $\mu\text{m}$ ) and K-band (1.96~2.46 $\mu\text{m}$ ) camera modules of IGRINS as a trial substitute for the full spectrograph cameras. The H-camera module indicated an F-number of 8.3 for 25.4 mm in diameter of input beam size, and 64 to 68 mm in diameter of lens sizes. Similarly, the K-camera module specified an F-number of 8.6 for 25.4 mm in diameter of input beam size and 68 to 81 mm in diameter of lens sizes. The achromatic lens used revealed an F-number of 8.0 for 25.4 mm in diameter of interferometer beam size and 50.8 mm in diameter of lens size. An optical performance of WFE was simulated by ZEMAX 12 Release 2 software.

### 2.1 Layout and flow diagram

The optical system consists of the achromatic lens, Dewar window and spherical lens as depicted in Fig. 1. Illumination at 633 nm in wavelengths from the interferometer passes through the Dewar entrance window, lens, Dewar exit window and reflects off the spherical mirror, and then goes back through in the reverse direction. The lens to be tested is located in a cryogenic Dewar box with window represented by the black dashed rectangle as shown in Fig. 1. The lens and spherical mirror have a specified  $\lambda/4$  surface irregularity and the Dewar window was manufactured with  $\lambda/50$  rms WFE. The lens was composed of BK7 and SF2.

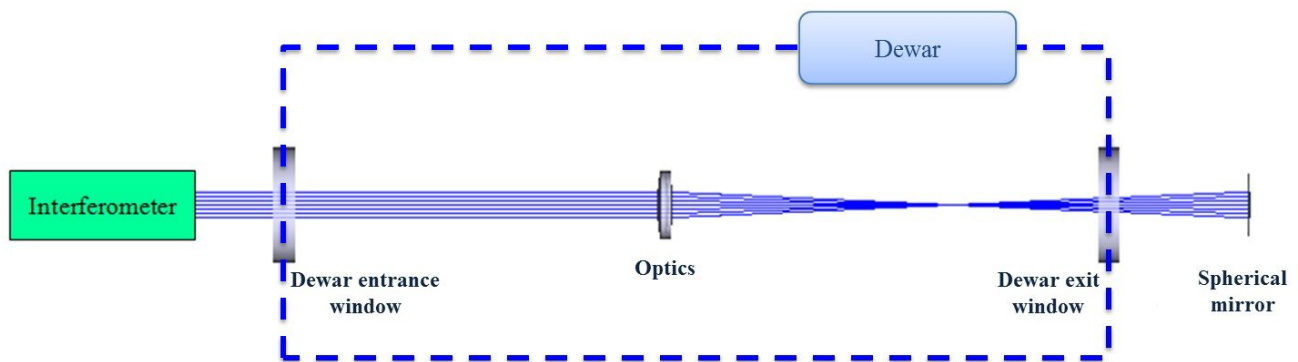


Figure 1. Optical layout for simulation

The conditions at RT and OT can be defined by 3 states as described in Fig. 2: room temperature / non-vacuum (RT/NV), room temperature / vacuum (RT/V) and operating temperature / vacuum (OT/V). In the 1<sup>st</sup> state of RT/NV, WFE simulation was carried out without any variation of physical property while the refractive index of air ( $n_a$ ) and  $rc$  of window were varied for the 2<sup>nd</sup> state of RT/V. For the 3<sup>rd</sup> state of OT/V,  $n_a$  should be replaced by the index at vacuum ( $n_0$ ) and  $rc$ ,  $t$  and  $dc$  of the lens were revised by temperature difference. Based on such a correlation, the WFE was simulated. The target rms WFE was set to less than  $0.01 \lambda$  to find the optimized minimum value and the corresponding

adjustment - tip, tilt, despace and decenter - quantities of the spherical mirror were substituted  $tip_0$ ,  $tilt_0$ ,  $despace_0$  and  $decenter_0$  for a reference position. From the reference, WFE criteria to obtain the perturbed adjustment quantities were less than  $0.03 \lambda$  rms WFE by giving a range of the quantities. Subscript n at the ranges represent an iteration number of tip, tilt, decenter and despace. For example, if the decenter quantity was adjusted from +1 to -1 mm with 0.1 mm step, number n is 21. The equivalent quantities for less than  $0.03 \lambda$  rms WFE were denoted by  $(tip_{min}, tip_{max})$ ,  $(tilt_{min}, tilt_{max})$ ,  $(despace_{min}, despace_{max})$  and  $(decenter_{min}, decenter_{max})$ .

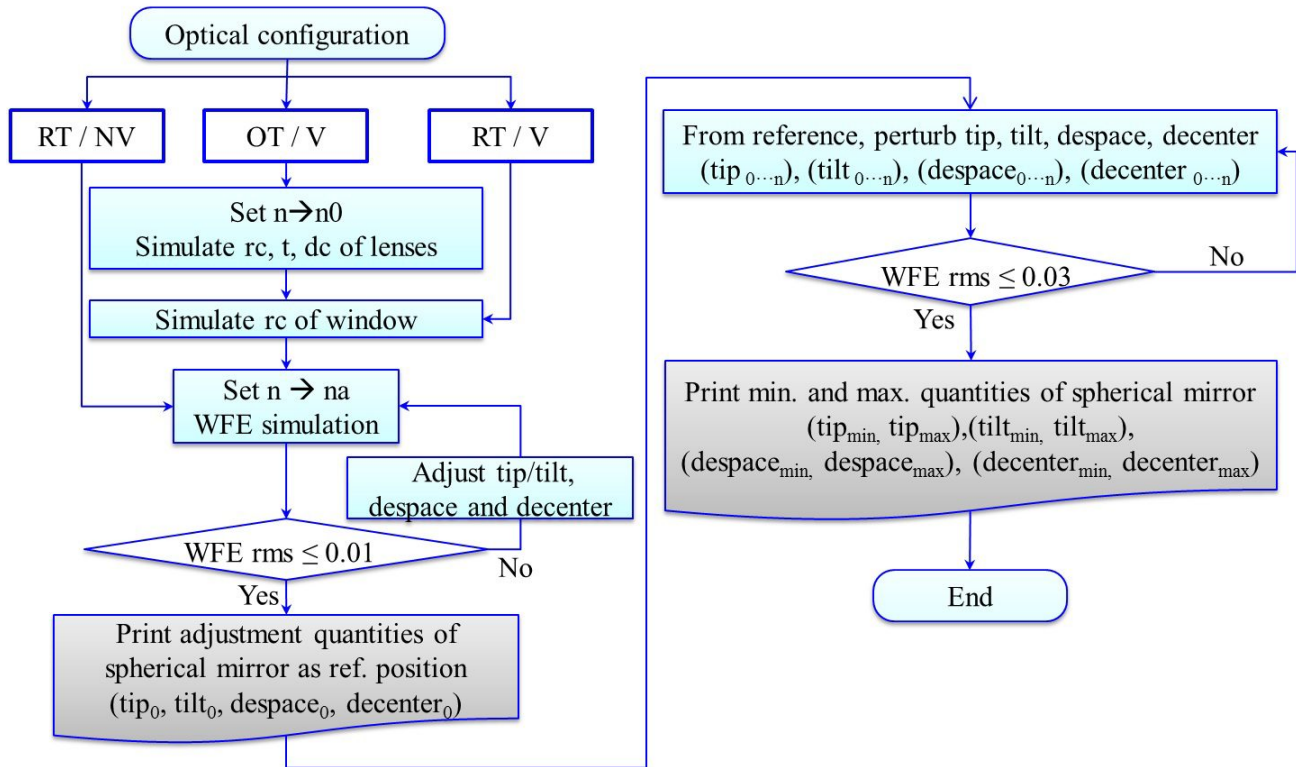


Figure 2. Flow diagram for simulation

## 2.2 Physical properties variation due to temperature change

The refractive index of the lens presents complicated nonlinear aspects with respect to temperature and wavelength diversity. Hence it is hard to obtain the corresponding index of refraction depending on varying temperatures for various lens materials. Due to insufficient information for the refractive index, approximate calculation was used in this simulation. Table 1 exhibits a variation of physical properties for different temperature and vacuum states. For the Dewar window, the simulation using Solidworks was fulfilled a by prediction of deformation under  $10^{-7}$  torr in pressure with 130 K of OT.

Table 1. Variation of physical properties due to environmental exchanges

States	RT/NV	OT/V	RT/V	remark
Lens refractive index ( $\lambda = 632.8 \text{ nm}$ )	N-BK7 : 1.51509 SF2 : 1.64379	N-BK7 : 1.51504 SF2 : 1.64401	-	NASA technical report <sup>23</sup>
Air refractive index	1.000273 ( <i>na</i> )	1.000000 ( <i>n0</i> )	1.000000 ( <i>n0</i> )	-

Lens curvature	R1 : 109.860 (CV) R2 : 93.110 (CV) R3 : 376.250 (CV)	R1 : 109.760 (CV) R2 : 93.00 (CV) R3 : 375.820 (CV)	-	RT: provided by vendor OT: simulated by SolidWorks CV: Convex
Lens thickness	N-BK7 : 8.50 SF2 : 2.00	N-BK7 : 8.49 SF2 : 1.99	-	contraction: 0.092 % (N-BK7) / 0.115 % (SF2)
Optical axis change with mount shrinking	-	-0.4 mm	-	contraction : -0.0033 %
Window curvature	Infinity	$1.8 \times 10^6$ mm	$1.8 \times 10^6$ mm	Window deformation: 1.65 $\mu$ m

Figure 3 depicts the surface deformation due to pressure differences. The maximum displacement is 1.65  $\mu$ m and the radius of curvature becomes  $\sim 1.8 \times 10^6$  m.

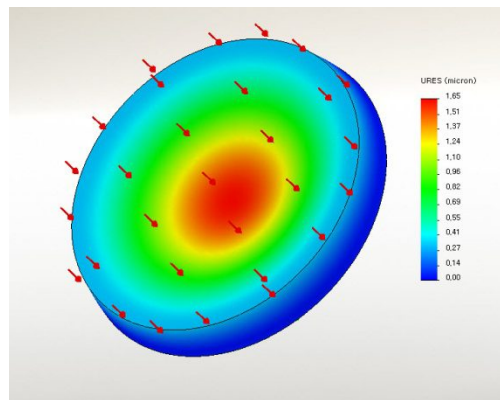


Figure 3. Window deformation in test Dewar due to pressure differences

A NASA technical report<sup>21</sup> gives the absolute index of refraction of N-BK7 through 0.5 to 2.5  $\mu$ m from 295 to 60 K. In the case of SF2, because measurement data were not available, the index was inferred from the values for SF15: Focusing on the fact that SF type material from Schott demonstrates a similar tendency in refractive index variation, we assumed the same rate of variation into SF2 where SF15 was cooled down from 295 to 130K for the diverse wavelengths.

Figure 4 displays the diversity of refractive index for both N-BK7 (Fig. 4 (a)) and SF15 (Fig. 4 (b)) at 0.6  $\mu$ m tailored on the data from NASA report<sup>21</sup>. According to the report, the maximum measurement uncertainty of refractive index was  $5.5 \times 10^{-5}$ . In Fig. 4 (a), the refractive index of N-BK7 decreases as temperature goes down from room temperature but it represents a minimum value at around 210 K and then an increase. SF15 reveals a different variation from N-BK7 as shown in Fig. 4 (b).

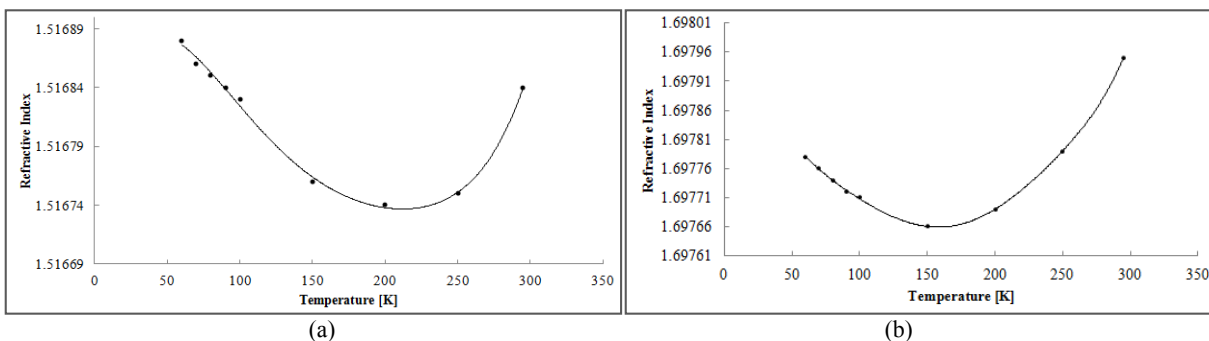


Figure 4. Refractive index changes with various temperatures for (a) N-BK7 and (b) SF15

The average Coefficient of Thermal Expansion (CTE) of the N-BK7 for 293-80 K was 5.65 ppm/K and the corresponding contraction rate should be 0.1203 % as reported by the GNIRS team<sup>24</sup>. Based on this tendency, the contraction rate of  $rc$  and  $t$  for the N-BK7 might be 0.092% for 293-130 K by linear interpolation. For the SF2, from the contraction rate<sup>22</sup> of both SF6 and SF57, the rate was calculated as 0.115 % at 130 K. The lens mount is composed of Aluminum and Stainless Steel 410 and the corresponding contraction rate stands for 0.327 % and 0.133 % at 130 K, respectively. Consequently, the optical axis of the lens becomes lower by about 0.4 mm in length than the original level as indicated in Table 1.

### 3. EXPERIMENTAL VERIFICATION

#### 3.1 Experimental procedure

The experiment was carried out with subsequent procedures as described in Fig. 5. We designed 3-dimensional modeling for the experimental setup before the preparation of optical components. The alignment was performed for all prepared components included in the interferometer, achromatic lens, spherical mirror and Dewar box. The WFE was measured while controlling temperature and pressure.

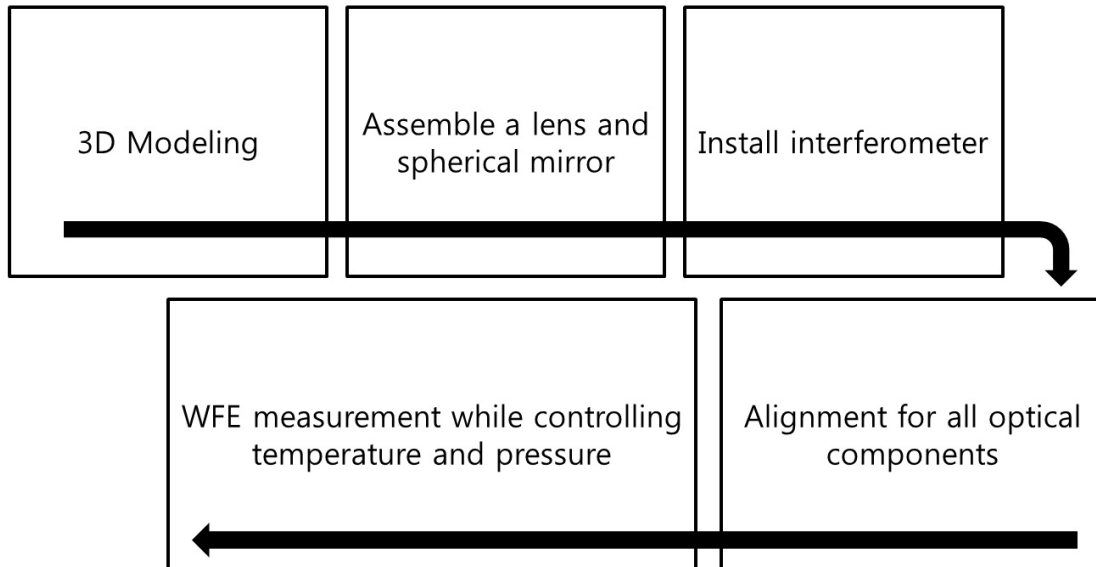


Figure 5. Experimental procedure

#### 3.2 Experimental setup

Figure 6 depicts the experimental setup in a class ~1000 clean room. The interferometer, achromatic lens, spherical mirror and Dewar were located on an optical table. Prior to assembling the Dewar box, the lens and mount were displayed as shown in Fig. 6 (a). These are the interferometer with 632.8  $\mu\text{m}$  of light source of PhaseCam 5030 from 4D Technology, achromatic lens assembly, spherical mirror assembly and vacuum pump from HiPace<sup>TM</sup> 80 of PFEIFFER Vacuum Corporation. The Dewar box was installed as depicted in Fig. 6 (b).

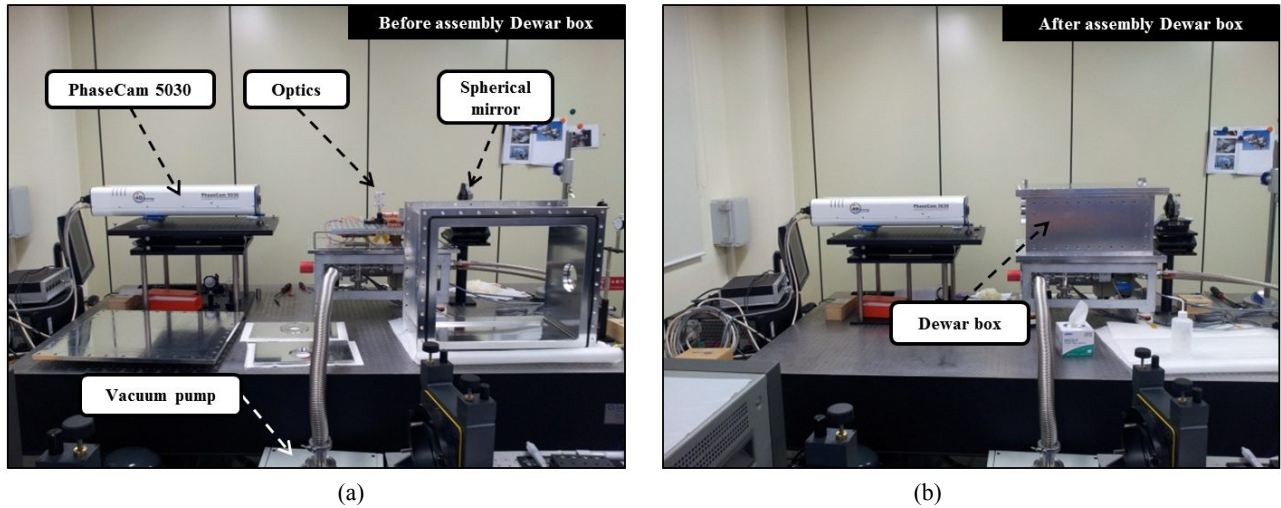


Figure 6. Experimental setup: (a) prior to assemble the Dewar box and (b) assembled the box

The photographs of the achromatic doublet lens with mount and spherical mirror with coordinate definition were shown in Fig. 7. In Fig. 7 (a), the copper clip was installed to prevent separation of the lens from the mount due to temperature variation. The spherical mirror was mounted on 2-axes linear stages and a lab jack, and coordinate definition was presented in Fig. 7 (b). The direction of the Z-axis coincides with the optical axis so that the axis was able to control despace. For the same reason, the Y-axis could be considered as the decenter direction. The mirror mount for the spherical mirror can also adjust tip and tilt using two knobs represented by a and b.

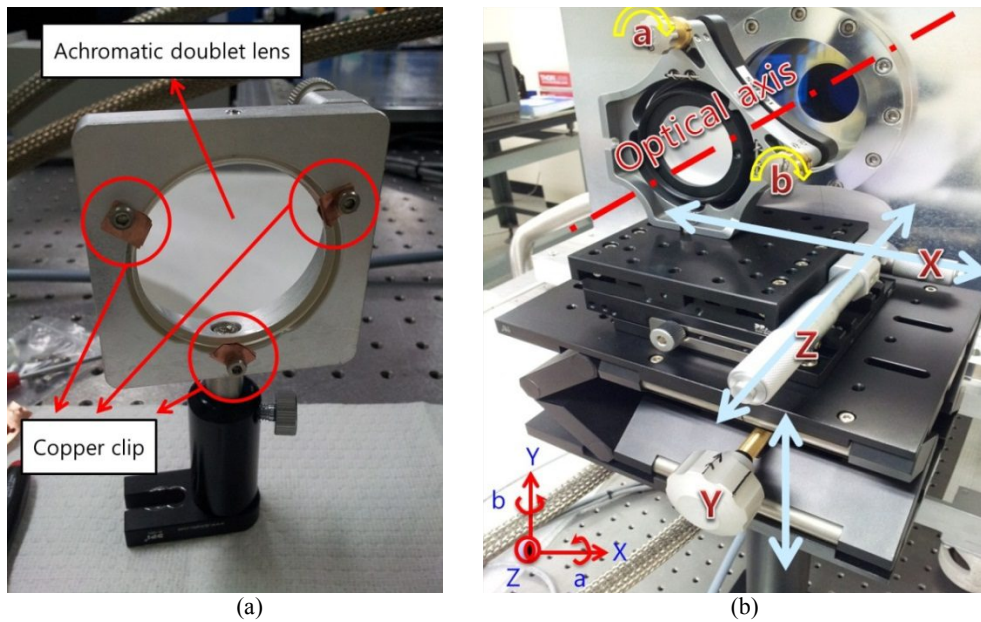


Figure 7. (a) Achromatic doublet lens with mount and (b) spherical mirror mount with coordinate definition

#### 4. RESULTS

The optical performance in the rms WFE unit for RT/NV state was predicted by the developed simulation flow presented in Chapter 2. In the Table 2, the range of predicted WFE was from 0.016 to 0.023 at the RT/NV state. The rms WFE was measured as 0.021 at the RT/NV state. The experimental result was included in the range of prediction by simulation. The predicted rms WFE while adjusting spherical mirror by suggested decenter and despace quantity was ranged from 0.129 to 0.201, and corresponding Z (despace) and Y-axes (decenter) were 0.27-0.41 and 0.2-1.2 mm in length,

respectively. In the 1<sup>st</sup> experiment as summarized in Table 3, we set the target rms WFE as 0.14 and equivalent Z and Y-axes were 0.4 and 0.13, respectively. The measured despace (Z-axis) was included in predicted ranges but the decenter (Y-axis) was out of range in the predicted regime. However this was not so critical because our goal we sought to achieve in this experiment was reached not by the Z and Y-axes but by the target rms WFE, and the difference was not large. When we cooled down the Dewar, the predicted and measured rms WFEs without adjustment were 0.017-0.018 and 0.019, respectively. The difference is quite small, a quantity of less than 0.002  $\lambda$  rms WFE, and the developed simulation can be dealt with quite predictably.

In the 2<sup>nd</sup> experiment as represented in Table 4, we set the target rms WFE as 0.16 and corresponding Z and Y-axes were 0.53 and 0.27, respectively. The measured decenter (Y-axis) was included in predicted ranges but the despace (Z-axis) was out of range in the predicted scope. The measured rms WFE after cooled down was 0.018 and the difference was less than 0.001  $\lambda$  rms WFE.

Table 2. Simulated and the 1<sup>st</sup> experimental results

States	rms WFE [ $\lambda$ ]			Despace (Z) [mm]		Decenter (Y) [mm]	
	Prediction (P)	Experiment (E)	Difference	P	E	P	E
RT/NV	0.016~0.023	0.021	-	0	0	0	0
Suggested decenter and despace (Adjust mirror)	0.129~0.201	0.14	-	0.27~0.41	0.4	0.2~1.2	0.13
OT/V	0.017~0.018	0.019	+ 0.001 ~ 0.002	0	0	0	0

Table 3. Simulated and the 2<sup>nd</sup> experimental results

States	rms WFE [ $\lambda$ ]			Despace (Z) [mm]		Decenter (Y) [mm]	
	Prediction (P)	Experiment (E)	Difference	P	E	P	E
RT/NV	0.016~0.023	0.021	-	0	0	0	0
Suggested decenter and despace (Adjust mirror)	0.129~0.201	0.16	-	0.27~0.41	0.53	0.2~1.2	0.27
OT/V	0.017~0.018	0.018	0.0 ~ -0.001	0	0	0	0

## 5. CONCLUSION

The developed simulation provides predictable rms WFE at both RT and OT environments, and suggests decenter and despace displacement at RT condition before cooling down. The simulation results are very predictable with experimental data as shown in Table 3 and 4. In addition, the suggested decenter and despace quantities at RT by simulation were applied to mechanical adjustment, and optical performance at OT coincided well without any adjustment. Thus a ‘no adjustment’ philosophy was successfully applied to IGRINS by no adjustment at OT. The resulting prediction accuracy was less than 0.002  $\lambda$  rms WFE. We plan to apply our simulation flow to the actual IGRINS optical modules such as Input Relay Optics (IO), Slit-Viewing Camera (SVC), H- and K-camera. The simulation might be utilized to perfect alignment for the cryogenic infrared optical system with highly accurate predictability.

## REFERENCES

- [1] Lin, J., Long, F. and Zhang, W., "Study on computer-aided alignment method," Proc. SPIE 5638, 674-681 (2005).
- [2] Kim, S., Yang, H. S., Lee, Y. W. and Kim, S. W., "Merit function regression method for efficient alignment control of two-mirror optical systems," Optics Express 15, 8 (2007).
- [3] Kim, Y., Yang, H. S., Kim, S. W. and Lee, Y. W., "Alignment of off-axis optical system with multi mirrors using derivative of Zernike polynomial coefficient," Proc. SPIE 7433, 74330C (2009).
- [4] Kim, E. D., Choi, Y. W. and Kang, M. S., "Reverse-optimization alignment algorithm using Zernike sensitivity," Journal of the Optical Society of Korea 9, 2 (2005).
- [5] Leviton, D. B., Frey, B. J. and Kvamme, T., "High accuracy, absolute, cryogenic refractive index measurements of infrared lens materials for JWST NIRCcam using CHARMS," Proc. SPIE 5904, 59040O-1 (2005).
- [6] Kaneda, H., Onaka, T., Nakagawa, T., Enya, K., Murakami, H., Yamashiro, R., Ezaki, T., Numao, Y. and Sugiyama, Y., "Cryogenic optical performance of the ASTRO-F SiC telescope," Applied Optics 44, 32 (2005).
- [7] IGRINS team., "IGRINS\_alignemnt\_procedure\_v1.6\_2012-05-17," KASI (2012).
- [8] Navarro, R., Schoenmaker, T., Kroes, G., Oudenhuisen, A., Jager, R. and Venema, L., "JWST-MIRI spectrometer main optics design and mait results," Proceedings of the 7th ICSO (2008).
- [9] Glazenberg-Kluttig, A. W., Przygodda, F., Hanenburg, H., Morel, S. and Pel, J. W., "Realization of the MIDI cold optics," Proc. SPIE 4838, 1171-1181 (2003).
- [10] Perrin, G., Leinert, C., Graser, U., Waters, L. B. F. M. and Lopez, B., "MIDI, The 10  $\mu$ m interferometer of the VLT," EAS (2002).
- [11] Rio, Y., Lagage, P. O., Dubreuil D., Tourrette, T. and Dhenain, G., "VISIR : A mid infrared imager and spectrometer for the VLT," Proc. SPIE 3354, 615-626 (1998).
- [12] Navarro, R., Elswijk, E., Tromp, J., Kragt, J., Kroes, G. Hanenburd, H. ., "Precision mechanisms for optics in a vacuum cryogenic environment," ICSO (2010).
- [13] Tromp, N., Rigal, F., Elswijk, E., Kores, G., Bresson, Y. and Navarro, R., "MATISSE cold optics opto-mechanical design," Proc. SPIE 7734, 63 (2010).
- [14] Pragt, J. H., Brink, R. v. d., Kroes, G., Tropm, N. and Ochs, J. B., "Piezo-driven adjustment of a cryogenic detector," Proc. SPIE 7018, 70184N-1 (2008).
- [15] Roose, S., Cucchiaro, A. and Chambure, D. de., "Design of the cryo-optical test of the Planck reflectors," First international workshop on Test Philosophies, Standards, Methods and Quality for Space Systems (2003).
- [16] Dohlen, K., Origine, A. and Ferlet, M., "Optical alignment verification of the Herschel – SPIRE Instrument," SPIRE-LAM-PUB-002091
- [17] Insausti, M., Garzon, F., Rasilla, J. L., Blanche, P. A. and Lemaire, P., "Performances of NIR VPHGs at cryogenic temperature," Proc SPIE 7018, 70184T-1 (2008).
- [18] Suganuma, M., Imai, T., Katayama, H., Naitoh, M., Tange, Y., Yui, Y. Y., Maruyama, K., Kaneda, H., Nakagawa, T., Kotani, M., "Optical testing of lightweight large all-C/SiC optics," ICSO (2010).
- [19] Ryder, L. A., "Cryogenic test results of engineering test unit optical components of the Near Infrared Camera for the James Webb Space Telescope," Proc. SPIE 7010, 701010-1 (2008).
- [20] Taccola, M., Bagnasco, G., Barho, R., Caprini, G. C., Giampietro, M. D., Gaillard, L., Mondello, G. and Salvignol, J. C., "The Cryogenic Refocusing Mechanism of NIRSpec Opto-Mechanical Design, Analysis and Testing," Proc. SPIE 7018 (2008).
- [21] Frey, B. J., Leviton, D. B. and Madison, T. J., "Cryogenic temperature-dependent refractive index measurements of N-BK7, BaLKN3, and SF15 for NOTES PDI," NASA Technical Report, 20070018848 (2007).
- [22] GNIRS., "SDN013.02 – Coefficient of Thermal Expansion," NOAO, <http://www.noao.edu/ets/gnirs/SDN0013-02.htm>, (1999).